Version of Record: https://www.sciencedirect.com/science/article/pii/S0273117717300881
Manuscript_05bc3b3e7f1867dd5e778faa98a6e9c9

Suomi NPP VIIRS/DNB imagery of nightglow gravity waves from various sources over China

Chang Lai[a,*], Jia Yue[b,c], Jiyao Xu[d], William Straka III[e], Steven Miller[f], Xiao Liu[g,d]

[a] *School of Mathematics and Physics, Chongqing University of Posts and Telecommunications, Chongqing, China*

[b] *Atmospheric and Planetary Sciences, Hampton University, Hampton, Virginia, USA*

[c] *ESSIC, University of Maryland, College Park, USA*

[d] *State Key Laboratory of Space Weather, Center for Space Science and Applied Research, Chinese Academy of Sciences, Beijing, China*

[e] *Cooperative Institute for Meteorological Satellite Studies, University of Wisconsin-Madison, Madison, Wisconsin, USA*

[f] Cooperative Institute for Research in the Atmosphere, Colorado State University, Fort Collins, Colorado, USA

[g] College of Mathematics and Information Science, Henan Normal University, Xinxiang, China.

Abstract

Observation of atmospheric gravity waves provides critical insight to weather and climate researches. Some gravity waves survive middle-atmospheric filtering as they propagate upward to the mesopause region and disturb the nightglow emission layer near 90 km AMSL, making the waves visible to both ground and space sensors. Based on the high-resolution images obtained by Day/Night Band on NOAA/NASA Suomi National Polar-orbiting Partnership environmental satellite, four representative gravity wave events over China are analyzed. With the help of VIIRS thermal infrared brightness temperature and MERRA wind data, we surmise that these waves originated from orography, thunderstorm, typhoon and baroclinic, respectively. Nadir viewing satellite observations cover a wide area and unlike the surface-based perspective, do not suffer from cloud obscuration. These new observations over remote areas provide important guidance for future deployment of ground based camera systems in China.

Keywords: Gravity waves; Day/Night band; Mountain waves; Convection; Jets and fronts

* Corresponding author at: School of mathematics and physics, Chongqing University of Posts and Telecommunications, Chongqing, 40065, China
E-mail address: laichang@cqupt.edu.cn

1 Introduction

Gravity waves have attracted considerable research attentions over recent decades due to their central influence a number of important atmospheric circulations (Lindzen, 1981; Holton, 1982; Fritts and Alexander, 2003). Pioneering research work on gravity waves was performed by Hines (1960), who presents a theoretical and numerical formula describing their observed motion. Hines' theory suggests that gravity waves play an important role in the process of energy and momentum transport, turbulence generation and middle atmosphere circulation. Subsequent theoretical, numerical and observational studies were carried out in the following decades, detailed in the reviews of Fritts (1984) and Fritts and Alexander (2003).

When propagating from the troposphere toward the middle and upper atmosphere, the amplitude of gravity waves increases with height while the air density decreases with height. When wave amplitude reaches a critical point, wave breaking ensues, leading to turbulence/eddy dissipation in the middle atmosphere (Hodges, 1967). When gravity waves break into smaller-scale waves, the background flow gains momentum and energy. Through the vertical propagation and breaking process, gravity waves transport and redistribute the momentum from source region to the dissipation region (Mclntyre, 1981, Clark and Bergin, 1997). The atmospheric circulation responses to this external momentum source, and in turn weather and climate, are influenced both regionally and globally (McLandress et al., 2012). In the lower stratosphere, gravity waves induce nucleation of nitric acid trihydrate in polar

stratospheric clouds, which worsen springtime ozone loss (Eckermann et al., 2009). In the ionosphere, gravity waves can disturb the telecommunication signals (e.g., global position system) used in many aspects of daily life (Hernández-Pajares, 2006).

Despite the understood significance of gravity waves, the description of their influences in global scale atmospheric models is parameterized for general lack of observations. Hence, there is an urgent need for high-resolution measurements of gravity waves in order to help to constrain these parameterizations. The earliest observations of gravity waves were collected in 1960s, using the structure of rocket vapor trails to infer the motion of gravity waves in the middle and upper atmosphere (Kochanski, 1964). Aircrafts and balloons contributed to this data inventory in the 1970s (e.g., Rosenberg and Dewan, 1975; Azeem and Cadet, 1977). Over the Arctic, meteorological balloons were sent to the upper troposphere and lower stratosphere to record gravity wave motions (Whiteway and Duck, 1999). To gain a more comprehensive understanding of wave characteristics, Dean-Day et al. (1998) combine Meteorological Measurement System and Micro Wave Temperature Profiler to deduce intrinsic frequency, wavelength and other dominant features. The core issue with the historical data collections lies with sampling—single aircraft or ground-based observation covers only a small region, while gravity waves often propagate in a horizon distance of hundreds to thousands of km. A full description of gravity waves requires an observing system capable of spanning these scales.

Instruments onboard earth-viewing satellites offer a unique way to obtain global characteristics of gravity waves at the requisite scales of observation. Satellite-borne

radiometers have a nadir view from a satellite, and scan through a wide area. The GPS limb sounders offer a high vertical but low horizonal resolution(e.g, Melbourne et al., 1994), while the nadir viewing infrared detectors take advantage in horizontal resolution of 10 km (e.g., Sakanoi, 2011) at the cost of low vertical resolution. In the middle atmosphere, small changes to CO_2 emissions (measured as brightness temperatures at 15 and 4.3 μm,) show the presence of gravity waves which can be obtained by subtracting the background (Alexander and Barnet, 2007). When included on low earth orbiting satellites these measurements provide a global-scale observation of gravity waves. For example, the Atmospheric Infrared Sounder (AIRS) on NASA's Aqua satellite is sensitive to atmospheric temperature and suitable for large-scale gravity waves in the stratosphere (Alexander and Teitelbaum, 2007; Gong et al., 2012).

Airglow (or nightglow, specific to the nocturnal chemiluminescent processes) is a useful tracer for studying gravity waves in the mesopause because it dominates the nighttime visible light signal on moonless nights. Gravity waves propagating through (or ducted along) the mesopause can be observed through their modulation of the airglow, intensity owing to the local temperature and density perturbations caused by the wave passage. Gravity wave induced airglow structures globally-occurring phenomena, and have been documented in the northern hemisphere (Clairemidi et al., 1985), southern hemisphere (Armstrong, 1982), and even at polar latitudes (Taylor and Henriksen, 1989). Among the sources of the airglow emission are, such as atomic oxygen (577 nm at the altitude of 97±5 km, 630 and 636 nm, 200-300 km), molecular

oxygen (761.9nm and 864.5 nm, 95±5 km), excited hydroxyl (OH*, 500-4400 nm, 87±5km), and atomic sodium (589.0 nm and 589.6 nm, 92±5km) (Khomich et al., 2008). For the Day/Night Band spectral band pass, the OH* species is the strongest contributor (Miller et al., 2012).

Airglow (or nightglow, specific to the nocturnal chemiluminescent processes) is a useful tracer for studying gravity waves in the mesopause because it dominates the nighttime visible light signal on moonless nights. Gravity waves propagating through (or ducted along) the mesopause can be observed through their modulation of the airglow intensity owing to local temperature and density perturbations caused by the wave passage. Gravity wave induced airglow structures are globally-occurring phenomena, and have been documented in the northern hemisphere (Clairemidi et al., 1985), southern hemisphere (Armstrong, 1982), and even at polar latitudes (Taylor and Henriksen, 1989). Among the sources of airglow emission are atomic oxygen (577, 630, and 636 nm), molecular oxygen (761.9nm and 864.5 nm), excited hydroxyl (OH*, 500-4400 nm), and atomic sodium (589.0 nm and 589.6 nm). For the Day/Night Band spectral band pass, the OH* species is the strongest contributor (Miller et al., 2012).

Wide-field-of-view photography has been used successfully to image airglow gravity waves (Peterson and Kieffaber, 1973; Clairemidi et al., 1985). All-sky imagers provide an even broader view (Taylor et al., 1987; Nakamura et al., 2005) and enable local monitoring of the occurrence and propagation of mesospheric gravity waves (Smith et al., 2000). The structures observed include bands (Taylor et al., 1995),

ripples (Taylor and Hill, 1991) and concentric wave patterns (Yue et al., 2013). A ground-based all-sky camera system deployed in Colorado captured at least nine mesospheric concentric gravity wave events during 2003-2008 (Yue et al., 2009), launched primarily by warm-season convective activity over the Rocky Mountains and High Plains.

The Ionosphere, Mesosphere, upper-Atmosphere, and Plasmasphere mapping (IMAP) Visible and near-Infrared Spectral Imager (VISI) provided a first ability to observe the occurrence and horizontal motion of small-scale (wavelength<100 km) gravity globally from the space platform (Sakanoi et al., 2011). The imaging resolution of IMAP/VISI ranges from 16-50 km over a 600 km wide swath with fore/aft views at 45° off-nadir, enabling the detection of wavelengths down to about 30 km. By combining the observation of IMAP/VISI on the International Space Station (ISS) and an all-sky imager on the ground, Perwitasari et al. (2015) examine the origin and propagation of concentric gravity waves.

The Day/Night Band (DNB) visible/near-infrared sensor onboard the Suomi National Polar-orbiting Partnership (S-NPP) satellite is designed to sense the nocturnal environment (Lee et al., 2006; Miller et al., 2013). The DNB yields high-resolution (0.74 km; over an order of magnitude higher than IMAP/VISI) imagery of nightglow gravity waves as launched from various sources (Miller et al., 2015). The diverse array of potential gravity wave sources across China (e.g., Tibetan Plateau in western China, seasonal thunderstorm activity, and landfalling typhoons along the eastern shores), makes it an ideal region for the study these phenomena

using DNB imagery. The paper is organized as follows: In section 2, we briefly introduce the S-NPP satellite and its DNB sensor. In section 3 we show images of gravity waves in nightglow as excited by different sources and discuss their properties. Section 4 concludes the paper.

2 VIIRS/DNB on S-NPP

The NOAA/NASA S-NPP satellite was launched into a sun-synchronous polar orbit 834 km above the earth on 28 October 2011 as a risk-reduction mission for the future Joint Polar Satellite System (JPSS) constellation. The satellite has a period of 102 min and has a local time descending node of 0130 AM. Among its environmental sensor payloads is the Visible/Infrared Imaging Radiometer Suit (VIIRS)—a 22 band whisk-broom scanning imager with 22 narrowband channels sampling portions of the optical spectrum (0.4-12 μm). Included as a special sensor (with its own dedicated focal plane array) on VIIRS is the Day/Night Band, designed for high sensitivity to low-intensity visible/near-infrared light from 500 to 900 nm. It was discovered post-launch that on moonless nights the DNB could detect meteorological clouds illuminated by nocturnal light source (mainly form reflected nightglow; Miller et al., 2012), and details of its ability to characterize direct upwelling emissions from the nightglow followed (Miller et al., 2015). The high resolution of DNB imager (0.74 km) grants an opportunity to measure the horizontal wavelengths of small scale gravity waves.

As part of an ongoing operational polar-orbiting program, S-NPP (and

forthcoming JPSS members) with its high spatial resolution DNB nightglow imaging capability enables a sustained means to studying gravity waves above the stratosphere occurring globally. This continuity provides opportunities to couple the DNB with gravity wave observations from various other satellite systems. The NASA A-Train constellation (which includes Aqua) flies in the same orbital plane as S-NPP but at a slightly lower altitude (705 km vs. 834 km), meaning the A-Train will 'lap' S-NPP every 2-3 days. The periods of ground track conjunction offer a unique ability in this regard. In particular, combining the results of VIIRS/DNB and the Atmospheric Infrared Sounder (AIRS) on the Aqua satellite, Yue et al. (2014) report a multi-level simultaneous observation of concentric gravity waves from a nadir view. To study the ionosphere-atmosphere coupling, Azeem et al. (2015) compare simultaneous detections of one gravity wave event at three different levels: the stratosphere (as seen by AIRS), the mesosphere (as observed by VIIRS/DNB), and ionosphere (as derived from ground-based GPS receivers). Such gravity wave 'soundings' provide important insight on the vertical propagation of waves and specifically the momentum deposition profile that is so critical for understanding the role of these waves in driving the middle/upper-atmospheric circulation.

In this study, we focus on the DNB observations of various gravity wave phenomena occurring above China. As mentioned previously, the geography of China is extremely diverse, with maritime/coastal zones, significant topography, high deserts, and sweeping plains ranging across low to high-latitudes (from 18 to 53°). Gravity waves detected in the nightglow observations arise from different sources throughout

this expansive domain, including orographic, thunderstorm, typhoon, and mid-latitude baroclinic systems (jet and fronts). A secondary motivation to study nightglow across Chinese is to provide guidance for deployment of future ground imager systems. Xu et al. (2015) details the design and construction of a ground-based all-sky imager network in northern China. Using a local imager network covering 2000 km×1400 km area in this region, they can observe the evolution of concentric gravity waves measure the phase speeds and periods of these waves (Li et al. 2011), complementing the broad domain but poor temporal sampling of the current satellite systems. As the Chinese ground imager network continues to expand, the insights gained from the dual surface/satellite perspectives are expected to increase over time.

3 Observations

3.1 Mountain Waves

When airflow blows over mountains, the vertical displacement usually forms gravity waves on the downwind side of the flow. These waves are often seen in the troposphere, but have also been observed and modeled in the upper atmosphere for many years (Eckermann and Preusse, 1999; Alexander et al., 2009; McLandress et al., 2012). Even in the mesosphere, mountain waves are captured by all-sky imagers (Smith et al., 2009). Mountain waves have several impacts, including aircraft safety, energy transport in climate modeling as well as even possibly affecting ozone concentration in polar regions (Eckermann et al., 2009). Large mountain ranges (e.g., Andes and Himalaya) can cause disturbances in a large area resulting in a source of

waves. Sensors on satellites, such as VIIRS, can obtain a complete view of mountain waves. The high resolution in visible/infrared band and broad field of view of VIIRS allows for the mountain wave measurement.

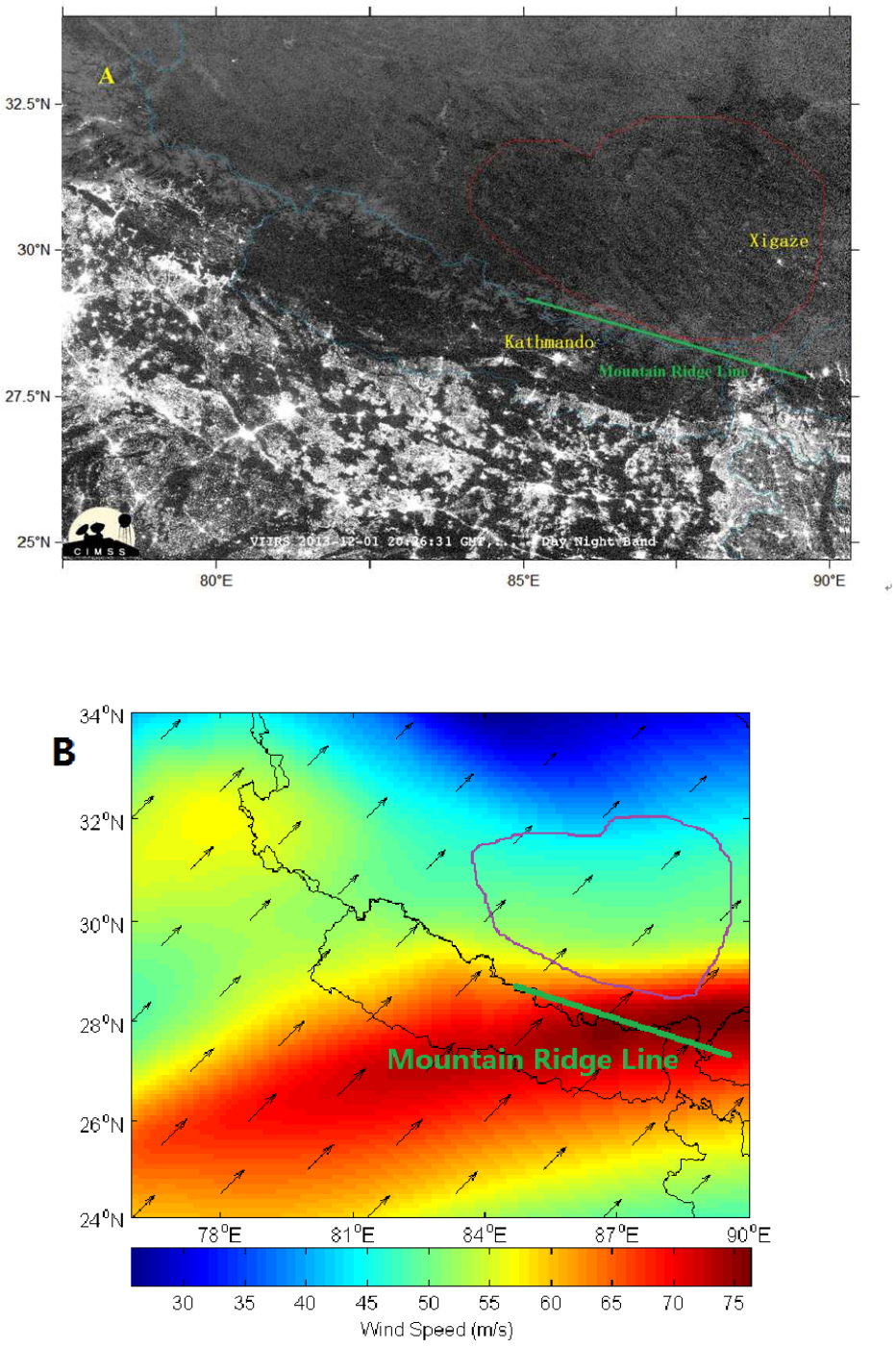

Fig. 1 Gravity waves and wind field over Tibet. (A) Gravity waves over Tibetan Plateau in

Day/Night Band visible/near infrared imagery on 1 December 2013 at 2026 UTC. Gravity waves with linear structure are enclosed by the red line and the Himalaya ridge is denoted by the green line. (B) MERRA wind field at 265.7 hpa on 1 December 2013 at 1800 UTC. The speed of south-westerly wind in the gravity wave area decreases from about 70m/s at south part to about 45m/s at north part.

Fig. 1(A) displays a gravity wave event near the ridge of Himalaya in western China. The DNB image was taken on the night of 1 December 2013, which was a waning crescent moon two days from the new moon. This means that the only light sources in the imagery shown is either from terrestrial light sources (agricultural fires and cities, such as those in India) or from nightglow. The Tibetan plateau is relatively unpopulated, meaning there are very few terrestrial light sources (Xigaze and Kathmandu, as marked). This means that the only emission over the Tibetan plateau is due to nightglow, meaning that the orographic induced mesospheric gravity waves are clearly visible. Regions to the south of the Tibetan plateau are lit up with terrestrial light sources (cities, agricultural fires) which mask the nightglow signature. The generation and vertical propagation of mountain waves strongly depend on the velocity of the background wind. In winter, the surface wind is more stable, which leads to a stronger mountain wave excitation. In addition, there is no wind reversal (zero wind) in winter background wind from the tropopause to the mesopause, making the vertical propagation of mountain waves to the upper atmosphere possible (Smith et al., 2009). The horizontal wavelength of gravity waves is about 23 km, which is estimated from Fig. 1(A) by averaging the intervals between several continuous clear

wave fronts.

Fig. 1(B) shows the wind field over Tibet and neighborhood, two and half hours before the S-NPP satellite captured the gravity wave event. The data of wind comes from the Modern-Era Retrospective Analysis for Research and Applications (MERRA), a climate satellites project undertaken by NASA (Rienecker et al., 2011). The wind speed at 265.7 hpa is about 57m/s in gravity wave area. The angle between the ridgeline and the south-westerly wind is about 62°. And the angle between wind and the propagation direction of gravity waves is about 10°. The direction of the wave fronts is changed by the wind and not longer parallel to the Himalayan ridgeline. VIIRS/DNB captured another gravity wave event on 3 May 2014 (Miller et al., 2015) in the same area. The gravity wave fronts in the picture taken on 3 May 2014 are parallel to the Himalayan ridgeline. These two gravity waves have the same linearly oriented train structure but different orientations.

The nadir-viewing satellite sensor provides a rare opportunity to observe mountain waves in southern Tibet. Because of the lack of light pollution from cities, the Tibetan plateau is an ideal location to set up ground-based all-sky imagers. Mountain waves have a unique character that they are fixed in space observed from ground and have small ground phase velocity. This cannot be easily determined from a single still satellite image, whereas ground-based all-sky airglow imagers can provide a time-elapsed observation to confirm the typical terrain-locked property of mountain waves. The ideal locations for the ground camera deployments are Nepal or Southern Tibet.

3.2 Thunderstorm generated gravity waves

Other than topography, convection is one of the main mechanisms to generate gravity waves in the lower atmosphere (Fritts and Alexander, 2003). The flow from overshooting tops, which occur in strong convection, disturbs the stably stratified air in the stratosphere (Pierce and Coroniti, 1966). This process results in a wide spectrum of gravity waves (Alexander et al., 1995). The large-scale waves can propagate up to the mesopause and beyond, travelling a large horizontal distance (Fritts and Alexander., 2003). The initial structure of waves remains when the wind speed and shear in the middle atmosphere is small (Taylor and Hapgood, 1988). The resulting mesospheric gravity wave signature appears as a series of expanding concentric rings, much like a pebble being dropped into a pond. In China, the most common time for intense convection occurs during the summer (Xu et al., 2015).

The mechanisms of thunderstorm generated gravity waves have been studied previously both in the aspects of model and observations. In model studies of convection, pure thermal forcing mechanism was applied by Salby et al. (1987), Alexander et al. (1995), Panya and Alexander. (1999), and then supported by McLandress et al. (2000) with observational evidence. The obstacle effect was suggested by Clark et al. (1986) and then developed by Pfister et al. (1993) and Vincent and Alexander. (2000); "mechanical oscillator" mechanism is presented by Fovell et al. (1992) and then described in a three-dimensional (3D) model by Lane et al. (2001).

Tayler and Hapgood (1988) revealed the thunderstorm as sources of concentric rings in nightglow using ground-based airglow imagers. There have been many other observations of convectively generated gravity waves from ground based airglow imagers in Shigaraki, Japan (Suzuki et al., 2007), the plains of Colorado in the United States (Yue et al., 2009) and finally in northern China (Xu et al., 2015) . Recently, these concentric gravity waves have been observed from VIIRS/DNB on S-NPP over intense convection in southern Texas (Miller et al., 2015) as well as other locations.

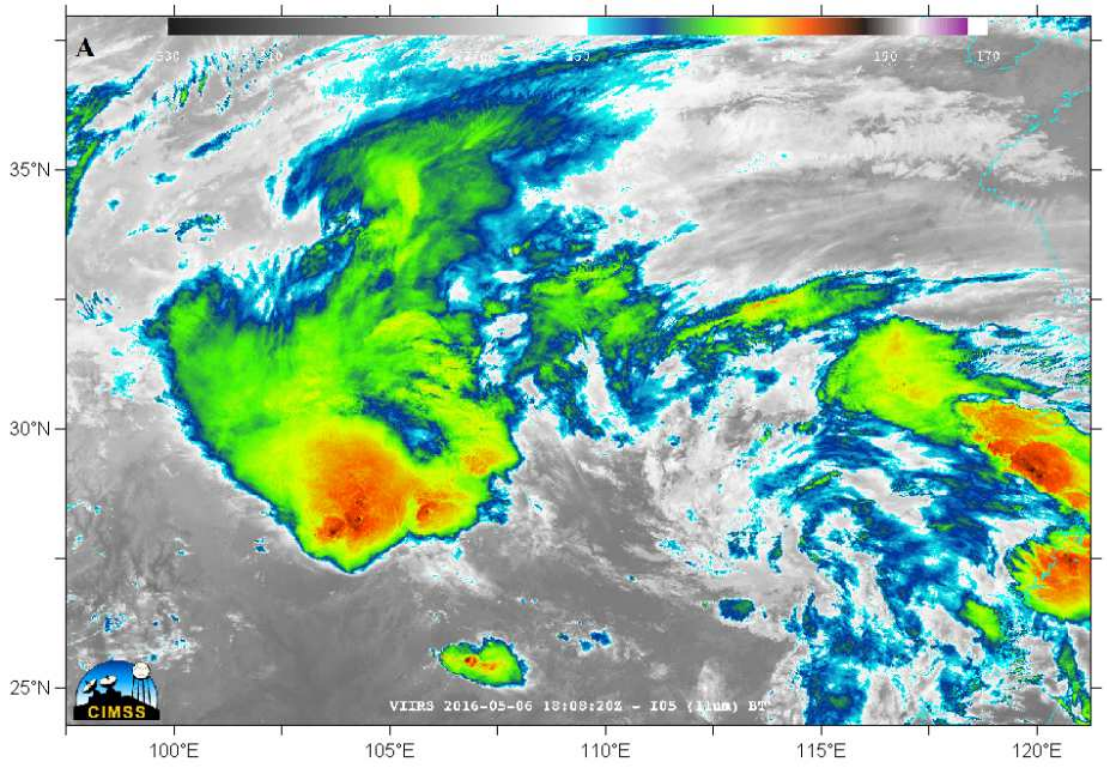

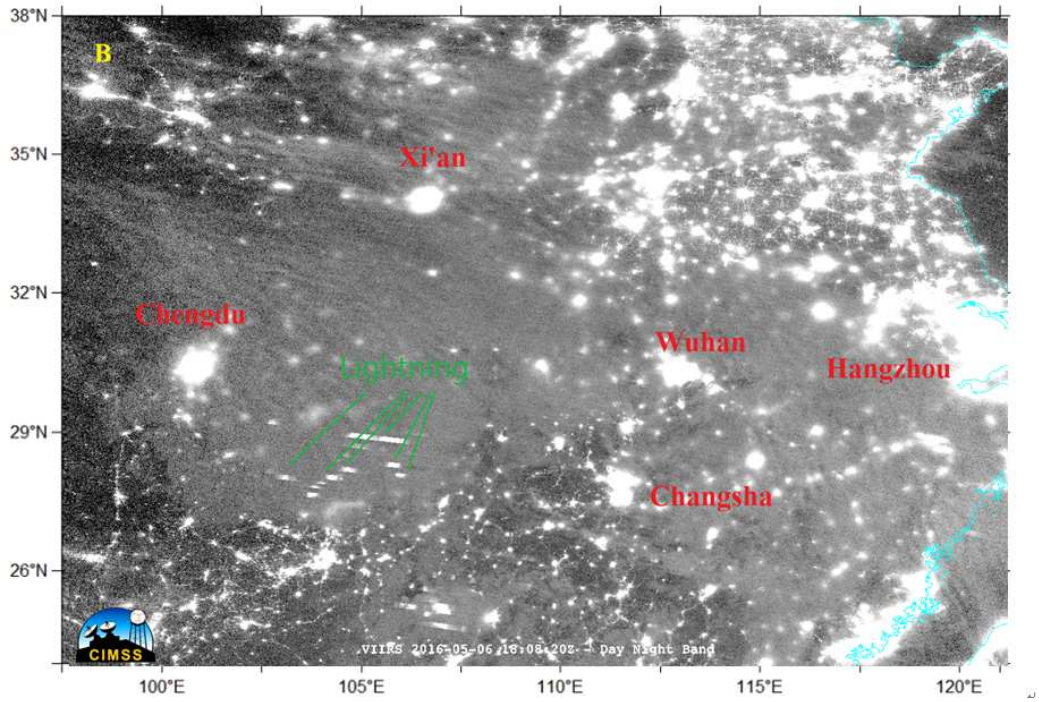

Fig. 2 (A) Concentric gravity waves excited by thunderstorms. VIIRS thermal infrared brightness temperature (11 μm) shows a thunderstorms in Sichuan, Southwest China, on 6 May 2016 at 1808 UTC. The deep convection overshooting the tropopause is indicated by the changing color (from red to black) at the center of storm cloud. The color bar indicates the brightness temperature ranges from 330 K (black) to 170 K (white). The temperature around the center of the storm is about 210 K (orange). (B) Corresponding nightglow imagery of the DNB. The concentric gravity waves caused by the storms at southwest spread widely over China. Major cities with bright city light are marked. The lightning flashes occurring during the DNB scans are shown as dashes.

One such other recent example was on 6 May, 2016 over northern China, where the DNB captured the concentric gravity waves initiated by storms, spreading in a wide area over northern China (Fig. 2). The wavelength of gravity waves measured from Fig. 2(B) varies from 16 to 30 km. The initial ring structure is not strictly preserved during the propagation (as shown in Fig. 2(B)). Due to the influence of background wind and wind shear, symmetry of concentric gravity waves was not

maintained and part of the waves appeared in arc pattern. In the report of Miller et al. (2015), the ripples of gravity waves generated by thunderstorms formed a series of concentric rings. In this situation, low wind speed and weak shear enable the waves to maintain the initial structure (Taylor and Hapgood, 1988).

Observing concentric wave from a single ground-based station is a challenge. An all-sky airglow observer covers a limited horizon circle of radius 420 km (Xu et al., 2015), which is not enough when observing the gravity waves with wavelengths longer than 200 km (Yue et al., 2013). Another obstacle is the cloudy weather near the ground camera, as clouds block the ability to view the nightglow rings from the ground. A network of ground-based stations can somewhat overcome the above difficulties and obtain comprehensive data of gravity waves with time elapse (Xu et al., 2015). From Figure 2, we can see that the future ground cameras can be installed away from the east coast to avoid bad weather, as well as light pollution from major cities, and observe convective gravity waves.

3.3 Typhoon gravity waves

A tropical cyclone (also called tropical storm, hurricane, typhoon, etc. depending on where it is located and the intensity) is a large, organized system of strong convection circulating around a low pressure system. These systems can generate upward-propagating gravity waves contributing to the globe circulation (Piani et al., 2000). Kim et al. (2005) used the three-dimensional mesoscale model (MM5) to study Typhoon Rusa (2002) and the characteristics of related gravity waves. Using the same

model, Kuester et al. (2008) simulated Hurricane Humberto and supported the obstacle mechanism of gravity wave excitation. Advanced Research Weather Research and Forecasting (WRF-ARW) modeling system (Skamarock et al., 2005) are also adapted by Kim and Chun (2010) to perform the simulation of Typhoon Saomai (2006) and associated gravity waves.

Gravity waves generated in the mesosphere can reach the height about 90 km and maybe higher, where OH* luminates and makes the gravity waves visible. This height is beyond the upper boundary of MM5 or WRF-ARW model. Observations at the nightglow layer are required to support the parameterization of upper atmosphere models. Using 3 ground based all-sky imagers, Suzuki et al. (2013) firstly reported typhoon generated gravity wave patterns in the mesopause region. Yue et al. (2014) presents a simultaneous spaceborne observation of tropical cyclone generated (similar to typhoons, but in the Indian Ocean) gravity waves in the stratosphere and mesosphere. Miller et al. (2015) captured the waves induced by Hurricane Ana with DNB imagery.

Figure 3 shows a gravity wave event associated with the Tropical Storm Fung-Wong over South China Sea on 19 September 2014. The tropical strom began on 13 September 2014 as a convectional cloudiness. As it intensified, to a tropical storm on 18 September 2014, the Japanese Meteorological Agency (the Regional Specialized Meteorological Centre for WMO region IV) named the system “Fung-Wong”. On the night of 19 September 2014 (local time), Fung-Wong made the landfall in Philippines. Figure 3 shows Tropical Storm Fung-Wong seen by the

VIIRS/DNB imager after landfall in the Philippines. The moon was a waning crescent moon five days from the new moon on 19 September, 2014 and below the horizon. This allowed nightglow features, such as the small-scale gravity waves over the southeastern part of the storm to be clearly observable. The horizontal wavelength is about 16 km. Unlike the concentric waves reported by Miller et al. (2015), the gravity waves are more linear likely due to wind shear and wave-absorbing wind layers. This observation helps to reveal the important dynamical effects of typhoon generated gravity waves. Because the tracks of typhoons in the western Pacific often take them close to the coast of China, airglow imagers placed there should be able to observe mesospheric gravity waves generated by typhoons.

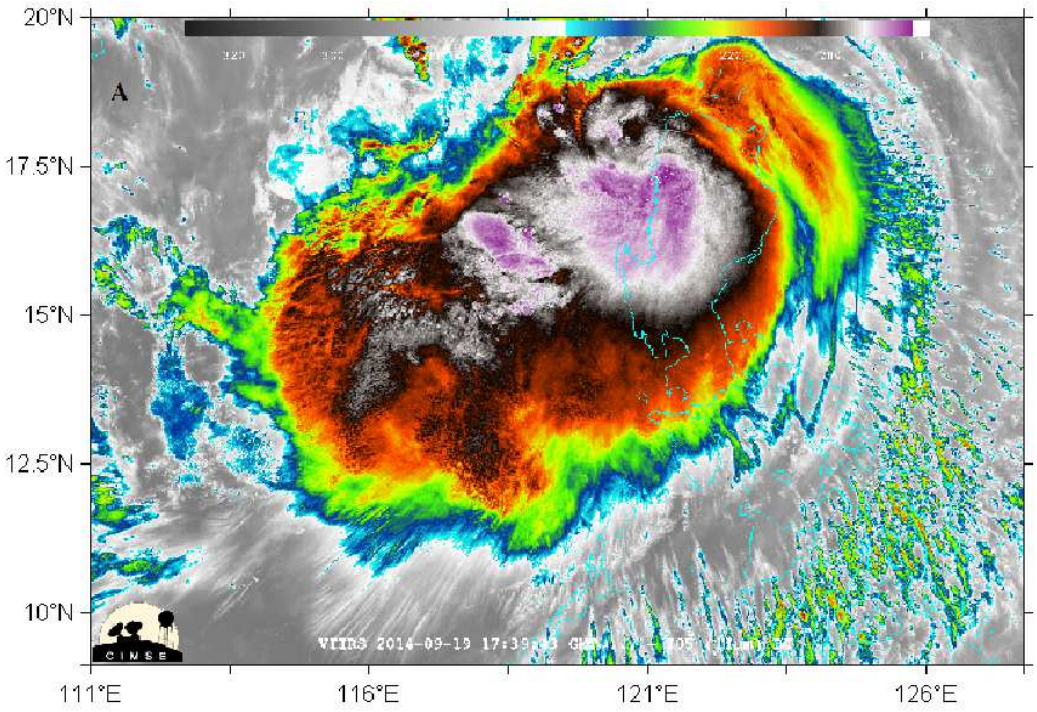

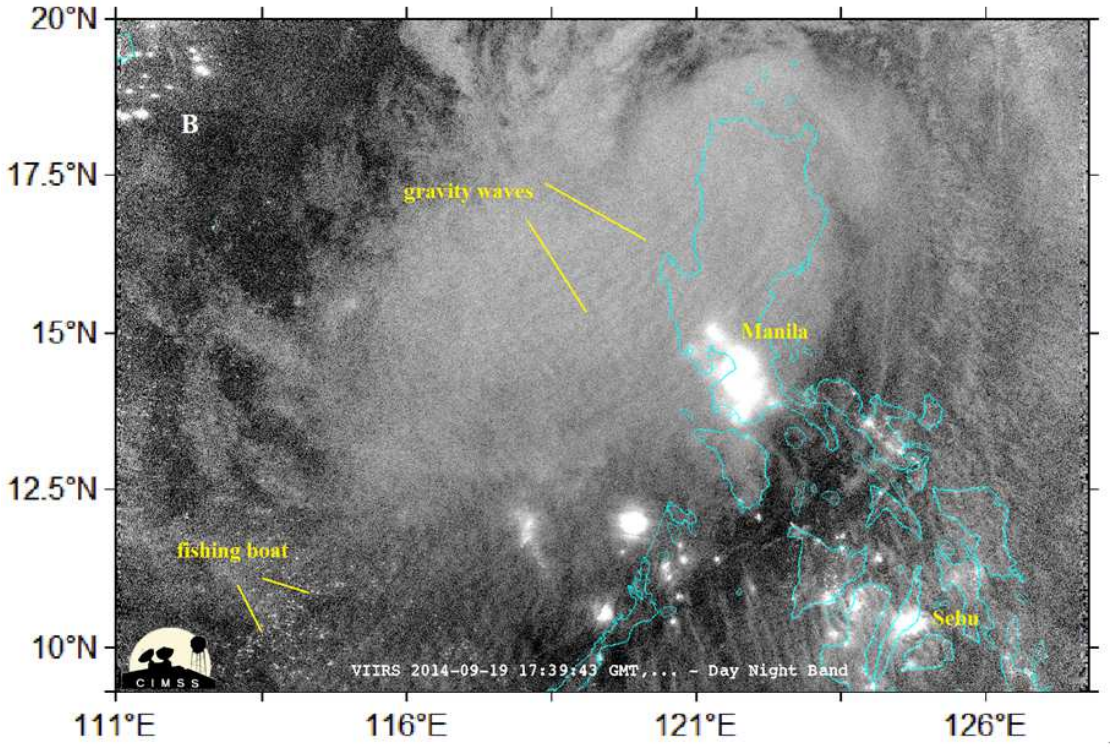

Fig. 3 Typhoon gravity waves of Fung-Wong over South China Sea. (A) VIIRS thermal infrared imagery shows Typhoon Fung-Wong on 19 September 2014 at 1739 UTC, in the northwest of Philippines. The color bar indicates the brightness temperature ranges from 330 K (black) to 180 K (white). The center of typhoon is about 190 K (purple). (B) Corresponding DNB imagery shows a series of linear wave patterns (noted by yellow line) in nightglow over the typhoon.

3.4 Gravity waves likely Jets and fronts induced

The main sources of gravity waves include orography, moist convection (e.g., thunderstorm and typhoon), jet instabilities, upper atmospheric dynamics, seismic and volcanic activity (Miller et al., 2015). Determining the source of a gravity wave event depends on the characters of the wave, orography and local weather condition.

Besides convection, jets and fronts are another important source of nonorographic waves. Gravity waves induced by jets and fronts contribute a lot to the energy and

momentum transfer, especially in the midlatitudes (Hertzog et al., 2008). The balance between the wind and other variables are used to approximate the gravity waves, for example, the simplest geostrophic balance (Zhang et al., 2000) and vertical hydrostatic balance (Vallis, 2006). The jets and fronts that generate gravity waves form a complex system, and the interaction between the gravity waves and the wind make the environment more complex (Plougonven and Zhang, 2014). More observations are needed to improve the understanding of the Jets and fronts induced gravity waves.

S-NPP satellite provides a reliable way to capture these waves. Fig. 4(A) shows a gravity wave event that occurs over the Taklamakan desert in the Tarim Basin of Xinjiang, China, located in northwest China on 3 November 2013. In this case, the moon was a new moon, meaning that the only sources of light observed in the DNB are terrestrial emission sources (fires, cities, aurora, etc.) or nightglow waves. In this case, the band patterns of nightglow over the dark area are obvious in the DNB image. The wave fronts are far away from and perpendicular to the local mountain ridge, which means that these are not generated by the local topography. In addition, there was no convection nearby, meaning that these waves were not induced by convection. The MERRA wind field at 265.7 hp is displayed in Fig. 4(B), from which we can see westerly tropospheric wind is along the transverse direction of the gravity waves. The wavelength is about 17 km. By comparing to the corresponding gravity waves source in Miller et al. (2015), we suggests two possible sources for these waves. They include an unstable jet, which is a possible candidate source, or secondary waves

generated by the primary wave breaking in the troposphere and stratosphere (Zhou et al., 2002). Because the Taklamakan desert is relatively unpopulated, new ground airglow imagers around northern Xinjiang (Southern Xinjiang is not populated) facing to the south, together with DNB, could characterize the gravity wave activities in Xinjiang and nearby mountains, deserts and Gobi.

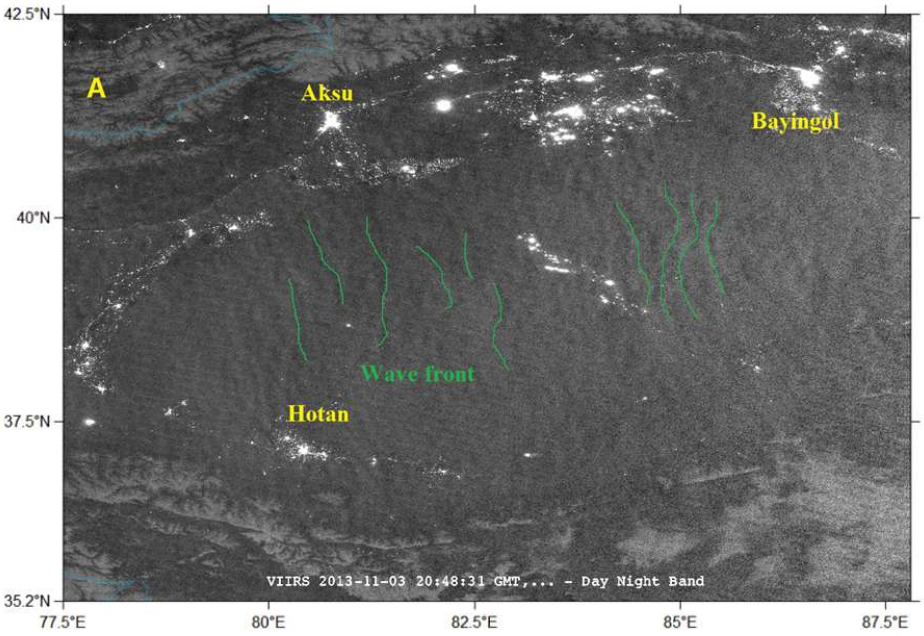

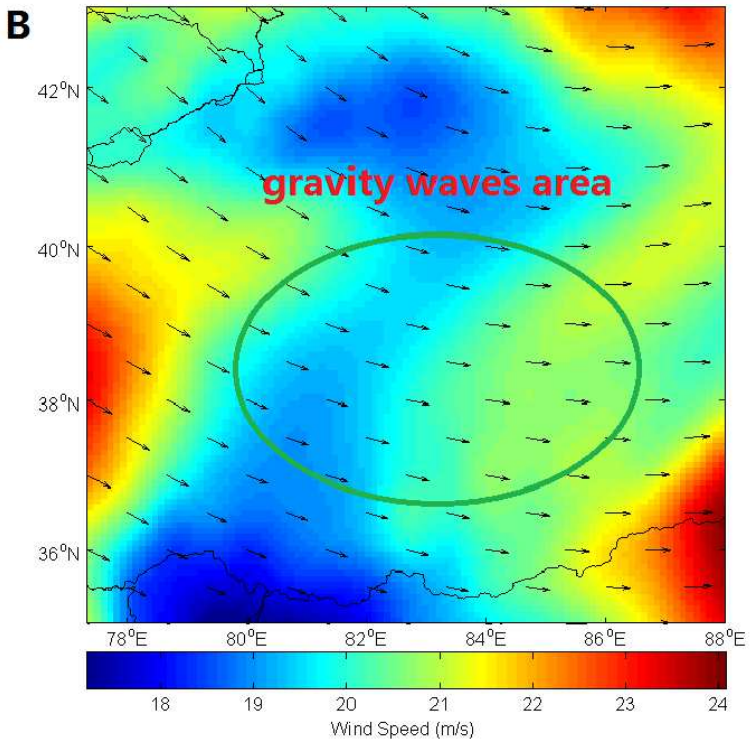

Fig. 4 Gravity waves over Xinjiang, China. (A) DNB imagery shows a gravity wave event on the night of 3 November 2013 at 2048 UTC (local time 0348 am). Major illuminated cities are denoted on the figure. Most area is dark in this area, which makes the gravity wave front obvious in the DNB imagery. The band patterns of nightglow are highlighted with green lines. (B) The MERRA tropospheric wind field at 265.7 hp, on the night of 3 November 2013 at 1800 UTC. The jet is perpendicular to the orientation of the gravity waves.

4 Conclusions

China has a wide area containing various terrain and weather features. Selected gravity waves triggered by different sources over China are discussed based on the VIIRS/DNB high resolution imagery. The nadir-viewing satellite sensor has a wide coverage and high spatial resolution, ignoring severe weather below. These advantages enable us to study the details of gravity waves from the satellite observation.

The spatial parameters, like horizontal wavelengths and shapes, can be measured by the satellite imagery. But due to Suomi NPP sun-synchronous orbit, its temporal sampling is rather poor. To obtain the wave speeds and periods, a ground based imager network is necessary, as being introduced in Xu et al. (2015). The capability of S-NPP satellite to observe nightglow gravity waves provide a helpful guidance for the development of future ground based cameras.

Acknowledgements

This research is partially supported by project 11547008 granted by NSFC. Chang Lai thanks the hosts of Hampton University and George Mason University and the Sponsorship of China Scholarship Council. The VIIRS Sensor Data Record data are distributed by the NOAA Comprehensive Large Array-data Stewardship System (CLASS).

References

Alexander, M. J., Holton, J. R., Durran, D. R., 1995. The gravity wave response above deep convection in a squall line simulation. J. Atmos. Sci. 52, 2212-2226.

Alexander, M. J., Barnet, C., 2007. Using satellite observations to constrain parameterizations of Gravity wave effects for global models. J. Atm. Sci. 64, 1652-1665.

Alexander, M. J., Teitelbaum, H., 2007. Observation and analysis of a large amplitude mountain wave event over the Antarctic peninusula. J. Geophys. Res. 112, D21103.

Alexander, M. J., Eckermann, S. D., Broutman, D., Ma, J., 2009. Momentum flux estimates for south Georgia island mountain waves in the stratosphere observed via satellite. Geophys. Res. Lett. 36, L12816.

Armstrong, E. B., 1982. The association of visible airglow features with a gravity wave. J.Atmos. Terr. Phys. 44, 325-336.

Azeeman, I., Cadet, D., 1977. Energy dissipation within intermittent clear air turbulence patches. J. Atmos. Sci. 34, 137.

Azeeman, I., Yue J., Hoffmann L., Miller S. D., Straka III W. C., Crowley G., 2015. Multisensor profiling of a concentric gravity wave event propagating from the troposphere to the ionosphere. Geophys. Res. Lett. 42, 7874-7880. doi:10.1002/2015GL065903.

Clairemidi, J., Herse, M., Moreels, G., 1985. Bi-dimensional obervation of waves near the mesppause at auroral latitudes. Planet. Space Sci. 33, 1013.

Clark T. L., Hauf T., Kuettner J. P., 1986. Convectively forced internal gravity waves: Results from two-dimensional numerical experiments, Q. J. R. Meteorol. Soc., 112, 899-925.

Clark, R. R., Bergin, J. S., 1997. Bispectral analysis of mesosphere winds. J. Atmos. Sloar-terr. Phys. 59, 629-639.

Dean-Day, J., Chan, K. R., Bowen, S. W., Bui, T. P., Gary, B.L., Mahoney, M. J., 1998. Dynamics of Rocky Mountain lee waves observed during SUCCESS. Geophys. Res. Lett. 25, 1351-1354.

Eckermann, S. D., Hoffmann, L., Höpfner, M, et al., 2009. Antarctic NAT PSC belt of June 2003: Observational validation of the mountain wave seeding hypothesis. Geophys. Res. Lett. 36, L02807.

Eckermann, S. D., Preusse, P., 1999. Global measurements of stratospheric mountain waves from space. Science 286, 1534-1537.

Fritts, D. C., 1984. Gravity wave saturation in the middle atmosphere: a review of theory and observations. Rev. Geophys., 22, 275-308.

Fritts, D. C., Alexander, M. J., 2003. Gravity wave dynamics and effects in the middle atmosphere. Rev. Geophys 41(1), 1003.

Fovell, R., Durran, D., Holton, J. R., 1992. Numerical simulations of convectively generated stratospheric gravity waves. J. Atmos. Sci. 49, 1427-1442.

Gong, J., Wu, D. L., and Eckermann, S. D., 2012. Gravity wave variances and propagation derived from AIRS radiances. Atmos. Chem. Phys. 12, 1701-1720.

Hernández-Pajares, M., Juan, J. M., Sanz, J., 2006. Medium-scale traveling ionospheric disturbances affecting GPS measurements: Spatial and temporal analysis. J. Geophys Res. 111, A07511.

Hertzog, A., Boccara, G., Vincent, R., Vial, F., Coquerez, P., 2008. Estimation of gravity wave momentum fluxes and phase speeds from long-duration stratospheric balloon flights. 2. Results from the Vorcore campain in Antarctica. J. Atmos. Sci. 65, 3056-3070.

Hines, C. O., 1960. Internal atmospheric gravity waves at ionospheric heights. Can. J. Phys. 38, 1441-1481.

Hodges, R. R., 1967. Generation of turbulence in the upper atmosphere by internal gravity waves. J. Geophys. Res. 72, 3455-3458.

Holton, J. R., 1982. The role of gravity wave induced drag and diffusion in the momentum bugget of the mesosphere. J. Atmos. Sci. 39(4), 791-799.

Kim, S. Y., Chun, H. Y., Baik, J. J., 2005. A numerical study of gravity waves induced by convection associated with Typhoon Rusa. Geophys. Res. Lett. 32, L24816.

Kim, S. Y., Chun, H. Y., 2010. Stratospheric gravity waves generated by Typhoon Saomai (2006): numerical modeling in a moving frame following the typhoon. J. Atmos. Sci. 67, 3617-3636.

Kochanski, A., 1964. Atmospheric motions from sodium cloud drifts. J. Geophys. Res. 69, 3651.

Kuester, M. A., Alexander, M. J., Ray, E. A., 2008. A model study of gravity waves over Hurricane Humberto (2001). J. Atmos. Sci. 65, 3231-3246.

Lane, T. P., Reeder, M. J., Clark, T. L., 2001. Numerical modeling of gravity wave generation by deep tropical convection. J. Atmos. Sci. 58, 1249-1274.

Lee, T. E., Miller, S. D., Joseph, F., Carl, C., 2006. The NPOESS VIIRS day/night visible sensor. bull. Am. Meteorol. Soc. 87, 191-199.

Li, Q., Xu, J., Yue, J., Yuan, W., Liu, X., 2011. Statistical characteristics of gravity wave activities observed by an OH airglow imager at Xinglong, in northern China. Ann. Geophys. 29, 1401-1410.

Khomich V. Y., Semenov A. I., Shefov N. N., 2008. Airglow as an indicator of upper atmospheric structure and dynamics. Berlin: Springer-Verlag.

Lindzen, R. S., 1981. Turbulence and stress owing to gravity wave and tidal breadsown. J. Geophys Res. 86(C10), 9707-9714.

McLandress, C., Alexander, M. J., Wu, D. L., 2000. Microwave limb sounder observations of gravity waves in the stratosphere: A climatology and interpretation. J. Gepphys. Res. 105, 11947-11967.

McLandress, C., Shepherd, T. G., Polavarpu, S., Beagley, S. R., 2012. Is missing orographic gravity wave drag near 60° S the cause of the stratospheric zonal wind biases in chemistry-climate models? J. Atmos. Sci. 69, 802-818.

Mclntyre, M. E., 1981, On the "wave momentum" myth. J. Fluid Mech. 106,331.

Melbourne, W. G., Davis, E. S., Duncan, C. B., et al., 1994. The application of spaceborne GPS to atmospheric limb sounding and global change monitoring. JPL Publ. 94-18.

Miller, S. D., Mills, S. P., Elvidge, C. D., et al., 2012. Suomi satellite brings to light a unique frontier of nighttime environmental sensing capabilities. Proc. Natl. Acad. Sci. 109, 15706-15711.

Miller, S. D., Straka III, W. C., Mills, S. P., et al., 2013. Illuminating the capabilities of the Suomi NPP VIIRS day/night band. Remote Sens. 5, 6717-6766.

Miller, S. D., Straka III, W. C., Yue J., et al., 2015. Upper atmospheric gravity wave details revealed in nightglow satellite imagery. Proc. Natl. Acad. Sci. 112, E6728-E6735.

Nakamura, T., Fukushima, T., Tsuda, T., et al., 2005. Simultaneous observation of dual-site

airglow imagers and a sodium temperature-wind lidar, and effect of atmospheric stability on the airglow structure. Adv. Space Res. 35, 1957–1963.

Pandya, R. E., Alexander, M. J., 1999. Linear stratospheric gravity waves above convective thermal forcing. J. Atmos. Sci. 56, 2434-2446.

Perwitasari, S., Sakanoi, T., Yamazaki, A., et al., 2015. Coordinate airglow observations between IMAP/VISI and a ground-based all-sky imager on concentric gravity wave in the mesopause. J. Geophys. Res. 120, 9706-9721.

Peterson, A. M., Kieffaber, L. M., 1973. Infrared photography of OH airglow structures. Nature 242, 321-322.

Pfister, L., Chan, K. R., Bui, T. P., et al. 1993. Gravity waves generated by a tropical cyclone during the STEP tropical field program: A case study. J. Geophys. Res. 98, 8611-8638.

Piani, C., Durran, D., Alexander, M. J., Holton, J. R., 2000. A numerical study of three-dimensional gravity waves triggered by deep tropical convection and their role in the dynamics of QBO. J. Atmos. Sci. 57, 3689-3702.

Pierce, A. D., Coroniti, S. C., 1966. A mechanism for the generation of acoustic-gravity waves during thunderstorm formation. Nature 210, 1209-1210.

Plougonven, R., Zhang, F., 2014. Internal gravity waves from atmospheric jets and fronts. Rev. Geophys 52, 33-76.

Rienecker, M. M., Suarez, M. J., Gelaro, R., et al., 2011. MERRA: NASA's modern-era retrospective analysis for research and applications, J. Climate 24, 3624-3648.

Rosenberg, N. W., Dewan, E. M., 1995. Stratospheric turbulence and vertical effective diffusion coefficients, Environ. Res., 535, 3, 1975. the ALOHA-93 campaign. Geophys. Res. Lett. 22, 2833-2836.

Salby, M. L., Garcia, R. R., 1987. Transient response to localized episodic heating in the tropics, Part I, Excitation and short-time near-field behaviour. J. Atmos. Sci. 44, 458-498.

Skamarock, W. C., Klemp, J. B., Dudhia, J., et al., 2005. A description of the advanced research WRF version 2. Technical Note NCAR/TN-486+STR, 88 pp., National Center for Atmospheric Research, Boulder, CO.

Sakanoi, T., Akiya, Y., Yamazaki, A., Otsuka, Y., Saito, A., Yoshikawa, I., 2011. Imaging observation of the Earth's mesosphere, thermosphere and ionosphere by VISI of ISS-I map on the international space station. IEEE Trans. Fundam. Mater 131, 983-988.

Smith, S. M., Mendillo, M., Baumgardner, J., Clark, R. R., 2000. Mesospheric gravity wave imaging at a subauroral site: First results from Millstone Hill. J. Geophys. Res. 105, 27119-27130.

Smith, S., Baumgardner, J., Mendillo, M., 2009. Evidence of mesospheric gravity-waves generated by orographic forcing in the troposphere. Geophys. Res. Lett. 36, L08807, doi:10.1029/2008GL036936.

Suzuki S., Shiokawa K., Otsuka Y., Ogawa T., Nakamura K., Nakamura T., A concentric gravity wave structure in the mesospheric airglow images. J. Geophys. Res. 112, D02012, 2007.

Suzuki S., Vadas S. L., Shiokawa K., Otsuka Y., Sawamura S., Murayama Y., Typhoon-induced concentric airglow structures in the mesopause region. Geophys. Res. Lett., 40, 5983-5987, doi:10.1002/2013GL058087, 2013.

Taylor M. J., Hapgood M. A., Rothwell P., 1987. Observations of gravity wave propagation in the OI (557.7nm), Na(589.2nm) and the near infrared OH nightglow emissions. Planet. Space Sci., 35, 413-327.

Taylor, M. J., Hapgood, M. A., 1988. Identification of a thunderstorm as a source of short period gravity waves in the upper atmospheric nightglow emissions. Planet space Sci. 36, 975-985.

Taylor, M. J., Henriksen, K., 1989. Gravity wave studies at polar latitudes, in Electromagnetic coupling in the polar clefts and caps. NATO ASI Series 278, 421-434.

Taylor, M. J., Hill, M. J., 1991. Near infrared imaging of hydroxyl wave structure over an ocean site at low latitudes. Geophys. Res. Lett. 18, 1333-1336.

Taylor, M. J., Turnbull, D. N., Lowe, R. P., 1995. All-sky measurements of short period waves imaged in the OI(557.7nm), Na(589.2nm) and near infrared OH and O_2(0,1) nightglow emissions during the ALOHA-93 campaign. Geophys. Res. Lett. 22, 2833-2836.

Vallis, G., 2006. Atmospheric and oceanic fluid dynamics, Cambridge Univ. Press, Cambridge, 745.

Vincent R. A., Alexander M. J., 2000. Gravity waves in the tropical lower stratosphere: An observational study of seasonal and interannual variability. J. Geophys. Res., 105, 17971-17982.

Whiteway, J. A., Duck, T. J., 1999. Enhanced Arctic stratospheric gravity wave activity above a tropospheric jet. Geophys. Res. Lett. 26,2453-2456.

Xu, J., Li, Q., Yue, J., et al., 2015. Concentric gravity waves over northern China observed by a n airglow imager network and satellites. J. Geophys. Res. Atm. 120, 11058-11078.

Yue, J., Vadas, S. L., She, C. Y., Nakamura, T., et al. 2009. Concentric gravity waves in the mesosphere generated by deep convective plumes in the lower atmosphere near Fort Collins, Colorado. J. Geophys. Res. 114, D06104.

Yue, J., Hoffmann, L., Alexander, M. J., 2013. Simultaneous observations of convective gravity waves from a ground-based airglow imager and AIRs satellite experiment, J. Geophys. Res. 118, 3178-3191.

Yue, J., Miller, D. M., Hoffmann, L., Straka III, W. C., 2014. Stratospheric and mesospheric concentric gravity waves over tropical cyclone Mahasen: joint AIRS and VIITS satellite observations. J. Atmos. Sol-Terr. Phy. 119, 83-90.

Zhou, X. L., Holton, J. R., Mullendore, G. L., 2002. Forcing of secondary waves by breaking of gravity waves in the mesosphere. J. Geophys. Res. 107(D7), doi:10.1029/2001JD001204.